Global glacial ice volume and Last Glacial Maximum duration from an extended Barbados sea level record

W.R. Peltier[a],*, R.G. Fairbanks[b]

[a]*Department of Physics, University of Toronto, Toronto, Ont., Canada M5S-1A*
[b]*Lamont-Doherty Earth Observatory and Department of Earth and Environmental Science Columbia University Palisades, NY 10964, USA*

Received 11 November 2005; accepted 25 April 2006

Abstract

Fundamental characteristics of the climate system during the most recent precessional cycle of the Earth's orbit around the Sun consist of the final expansion of land ice to its maximum extent, the subsequent episode of deglaciation, and the variations of global sea level that accompanied these events. In order to address the important issue of the variation of continental ice volume and related changes in global sea level through the late glacial period, we employ an extended set of observations of the pre-glacial and postglacial history of sea-level rise at the island of Barbados, together with a refined model of continental deglaciation and an accurate methodology for the prediction of postglacial sea-level change. Although our results provide unambiguous evidence that the post LGM rise of eustatic sea-level was very close to the widely supported estimate of 120 m, the data also provide evidence that LGM must have occurred 26,000 years ago, approximately 5000 yr earlier than the usually assumed age.

© 2006 Published by Elsevier Ltd.

1. Introduction

Analysis of Oxygen Isotope dilution histories derived from mass spectrometric measurements on the tests of forminifera extracted from deep sea sedimentary cores provide a means whereby one may estimate the amount by which globally averaged sea-level was lower than present at LGM (Shackleton, 1967; Chappell and Shackleton, 1986; Shackleton, 2000). This is a simple consequence of the fact that an isotopic fractionation accompanies the growth of land ice such that the residual ocean is isotopically enriched in $H_2^{18}O$. Application of this method delivers the generally accepted estimate that sea level was lower at LGM by approximately 120 m. However, there is uncertainty in this estimate due to isotopic influences of changing bottom water temperatures (e.g. see Adkins et al., 2002) and uncertainties in the mean isotopic composition of continental ice through time (Mix and Ruddiman, 1984). Since direct measurements of the actual LGM low stand of the sea, at sites sufficiently distant from the major centers of

continental glaciation, confirm that sea level was indeed lower by approximately this same amount (Fairbanks, 1989; Hanebuth et al., 2000), it would appear that the $\delta^{18}O$-based inference is rather robust in spite of these uncertainties. The observed depression of LGM sea-level at the island of Barbados in the Caribbean Sea is especially important in this regard as it has been shown (Peltier, 2002a,b,c) that sea-level history at this single location provides a very good approximation to the globally averaged ice equivalent (eustatic) history of postglacial sea-level change.

In spite of this accord between the direct and isotopically derived estimates of the LGM depression of eustatic sea-level, a third line of argument based upon use of a theory of postglacial relative sea level (RSL) change has recently been invoked to suggest that the eustatic LGM low stand could have been as much as 135 m or more below present sea level (Yokoyama et al., 2000; Lambeck and Chappell, 2001). The validity of this estimate has recently been supported by an independent analysis (Mitrovica, 2003) in which the eustatic depression is asserted to lie between 130 and 135 m. At the heart of this line of reasoning is an argument concerning the manner in which one should calculate RSL history in a region in which a broad

---
*Corresponding author. Tel.: +1 416 978 2938; fax: +1 416 978 8905.

E-mail addresses: peltier@atmosp.physics.utoronto.ca (W.R. Peltier), fairbanks@ldeo.columbia.edu (R.G. Fairbanks).

continental shelf is exposed by the fall of sea-level during glaciation and later inundated by the sea during deglaciation, and an assumption concerning the data that may be employed to constrain such analysis. Although it has been demonstrated in Peltier (2002a,b) that the original mathematical analysis described in Yokoyama et al. (2000) was seriously flawed, the conclusion itself has not been withdrawn. This is in spite of the fact that the authors have published a retraction of the methodology employed (Yokoyama et al., 2001). One purpose of this Article is to contribute to the resolution of this important debate. To this end we will first focus upon a newly augmented and refined RSL data set from the critical Barbados location.

1.1. The Barbados record of postglacial sea-level history

The island of Barbados, located in the eastern Caribbean Sea, approximately 150 km east of the Lesser Antilles, at 13°5′N. latitude and 59°32′W. longitude (Fig. 1), is a site from which an especially accurate U/Th dated coral-based record of postglacial RSL history has been available for some time (Fairbanks, 1989; Bard et al., 1990). Also shown in Fig. 1 are the locations of the main concentrations of land ice that existed at LGM according to the recently constructed ICE-5G (VM2) model (Peltier, 2004), and the locations of several sites from which accurate records of Holocene sea-level history are available that will be discussed in what follows. The original data set from Barbados has been significantly augmented (Fairbanks et al., 2005) since publication of these seminal accounts and the newly available complete data set is listed in Table 1 and plotted in Fig. 2, where the new data are denoted by purple symbols and the original data by green. The basic wireline core stratigraphy for all samples reported in this paper can be found in Fairbanks (1989) and sample descriptions and locations are presented in Fairbanks (1988). In plotting these data we have adjusted the depths from which the individual coral samples were actually recovered to account for an assumed constant rate of tectonic uplift of $0.34\,\mathrm{mm\,yr^{-1}}$ (Fairbanks, 1989) and also
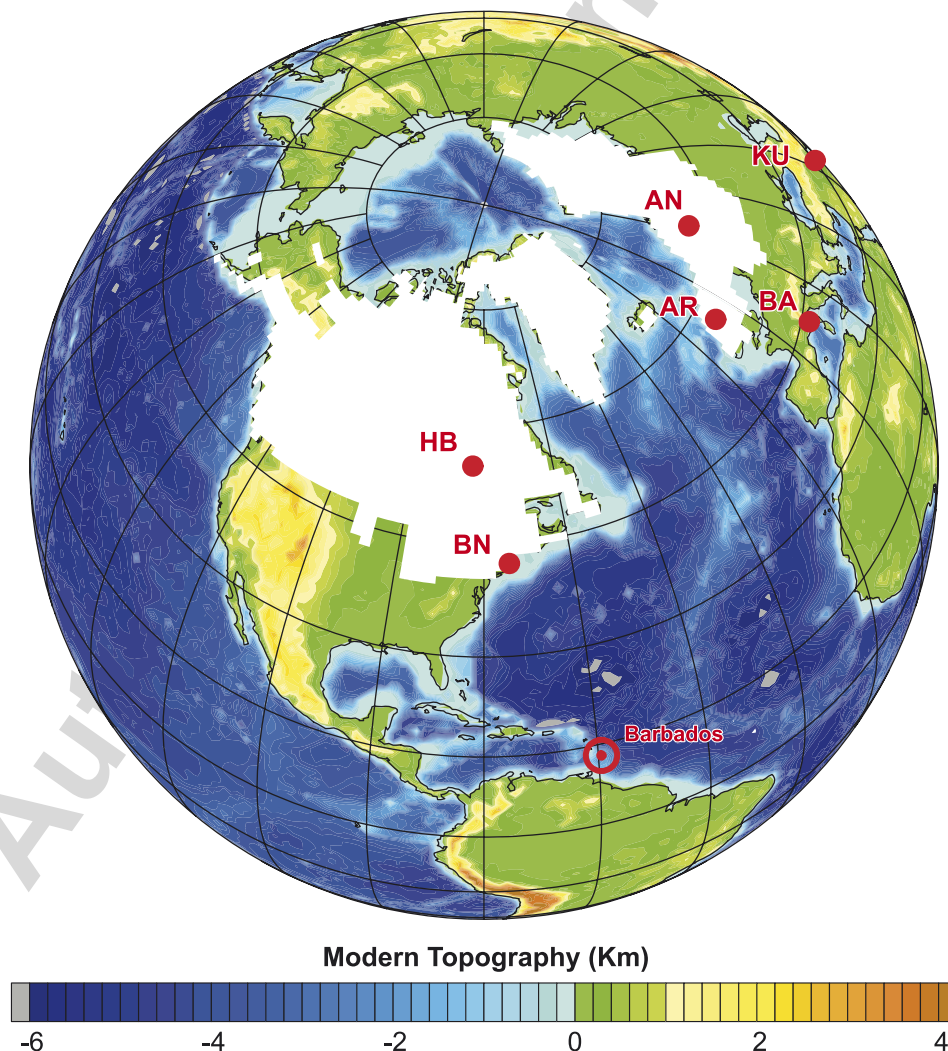

Fig. 1. Location of the Island of Barbados and several other sites from which relative sea-level records are available together with the location of the northern hemisphere continental ice sheets that existed at Last Glacial Maximum.

Table 1

Sample	Location	Species	Depth (m)	Depth(m) uplift corrected	Mean Th/U Age yr BP	Mean 1 sig U-Th
RGF B56	Barbados	*A. palmate*	1	1.3	726	10
RGF 7-5-5	Barbados	*A. palmate*	18.5	21.4	9930	17
RGF 7-9-6	Barbados	*A. palmate*	21.61	24.7	8936	22
RGF 7-10-2	Barbados	*A. palmate*	22.27	25.4	8934	30
RGF 7-12-2	Barbados	*A. palmate*	25.43	28.6	9155	18
RGF 7-16-2	Barbados	*A. palmate*	30	33.3	9618	23
RGF 7-16-6	Barbados	*A. palmate*	30.24	33.6	9922	21
RGF 7-19-3	Barbados	*A. palmate*	33.1	36.5	9941	33
RGF 7-23-4	Barbados	*A. palmate*	37.76	41.4	10571	39
RGF 7-26-2	Barbados	*A. palmate*	39.08	42.8	10808	23
RGF 7-27-4	Barbados	*A. palmate*	40.7	44.5	11078	37
RGF 9-8-2	Barbados	*A. palmate*	88.6	93.5	14082	28
RGF 9-9-7	Barbados	*A. palmate*	89.51	94.4	14295	29
RGF 9-11-2	Barbados	*A. palmate*	90.75	95.6	14255	20
RGF 9-12-5	Barbados	*A. palmate*	92.49	97.4	14408	20
RGF 9-12-7	Barbados	*A. palmate*	92.57	97.5	14396	18
RGF 9-13-3	Barbados	*A. palmate*	93.89	98.9	14539	23
RGF 9-20-2	Barbados	*A. palmate*	105.2	111.4	18116	37
RGF 9-21-6	Barbados	*A. palmate*	105.81	112.0	18174	33
RGF 9-21-9	Barbados	*A. palmate*	105.93	112.2	18448	50
RGF 9-21-10	Barbados	*A. palmate*	105.93	112.2	18218	44
RGF 9-21-11	Barbados	*A. palmate*	106.09	112.2	18176	56
RGF 9-22-4	Barbados	*A. palmate*	106.9	113.2	18549	26
RGF 9-23-2	Barbados	*A. palmate*	107.33	113.7	18746	64
RGF 9-23-5	Barbados	*A. palmate*	107.49	113.9	18783	80
RGF 9-24-2	Barbados	*A. palmate*	109.09	115.5	18716	28
RGF 9-24-4	Barbados	*A. palmate*	109.26	115.7	18806	33
RGF 9-27-5	Barbados	*A. palmate*	113.81	120.3	19075	55
RGF 12-5-2	Barbados	*A. palmate*	53.04	56.9	11392	22
RGF 12-6-7	Barbados	*A. palmate*	54.66	58.6	11511	37
RGF 12-9-3	Barbados	*A. palmate*	57.43	61.5	12002	25
RGF 12-9-5	Barbados	*A. palmate*	57.59	61.8	12203	38
RGF 12-9-6	Barbados	*A. palmate*	57.74	61.9	12170	15
RGF 12-12-2	Barbados	*A. palmate*	60.42	64.8	12798	25
RGF 12-14-4	Barbados	*A. palmate*	62.26	66.6	12844	39
RGF 12-15-4	Barbados	*A. palmate*	63.78	68.2	12993	17
RGF 12-16-5	Barbados	*A. palmate*	65.36	69.8	13088	56
RGF 12-17-2 CL	Barbados	*A. palmate*	65.78	70.3	13179	16
RGF 12-21-2	Barbados	*A. palmate*	69.06	73.7	13555	19
RGF 12-21-6	Barbados	*A. palmate*	69.35	74.0	13574	26
RGF 12-21-7	Barbados	*A. palmate*	69.57	74.2	13578	26
RGF 12-21-10	Barbados	*A. palmate*	69.85	74.5	13632	16
RGF 12-28-6	Barbados	*A. palmate*	77.44	87.5	29540	41
RGF 12-28-7	Barbados	*A. palmate*	77.56	87.8	30147	57
RGF 12-29-2	Barbados	*A. palmate*	77.92	88.2	30225	75
RGF 12-30-2	Barbados	*A. palmate*	78.46	88.8	30298	110
RGF 12-30-3	Barbados	*A. palmate*	78.56	88.9	30242	48
RGF 13-8-9	Barbados	*A. palmate*	105.95	111.9	17580	69
RGF 15-5-3	Barbados	*A. palmate*	91.34	96.3	14573	15
RGF15-9-5	Barbados	*A. palmate*	101.63	107.9	18408	26
RGF 15-10-1	Barbados	*A. palmate*	101.69	108.3	19392	29
RGF 15-12-2	Barbados	*A. palmate*	103.18	109.9	19518	33
RGF 15-12-5	Barbados	*A. palmate*	103.56	110.3	19708	26
RGF 16-12-6	Barbados	*A. palmate*	54.3	58.2	11512	17
RGF 16-12-7	Barbados	*A. palmate*	54.41	58.3	11391	36
RGF 9-1-2	Barbados	*M. annularis*	78.08	82.2	12179	33
RGF 9-1-6	Barbados	*M. annularis*	78.33	82.4	12029	30
RGF 9-1-7	Barbados	*M. annularis*	78.43	82.5	11774	41
RGF 9-1-8	Barbados	*M. annularis*	78.74	82.9	12212	64
RGF 9-2-3	Barbados	*M. annularis*	79.63	83.7	12016	28
RGF 9-2-5	Barbados	*M. annularis*	80.01	84.1	12103	39
RGF 9-2-7	Barbados	*M. annularis*	80.24	84.4	12309	36

Table 1 (*continued*)

Sample	Location	Species	Depth (m)	Depth(m) uplift corrected	Mean Th/U Age yr BP	Mean 1 sig U-Th
RGF 9-3-2	Barbados	*M. annularis*	81.15	85.4	12303	14
RGF 9-3-4	Barbados	*M. annularis*	81.48	85.8	12680	75
RGF 9-35-6	Barbados	*M. annularis*	125.68	133.2	22160	62
RGF 9-37-2	Barbados	*M. annularis*	126.82	134.5	22536	46
RGF 9-37-3	Barbados	*M. annularis*	127	134.7	22574	48
RGF 9-38-1	Barbados	*M. annularis*	128.62	136.5	23044	37
RGF 9-38-2	Barbados	*M. annularis*	128.78	136.7	23296	61
RGF 9-38-3	Barbados	*M. annularis*	128.85	136.7	23039	38
RGF 9-39-2	Barbados	*M. annularis*	129.94	138.1	23867	44
RGF 9-39-3	Barbados	*M. annularis*	130.05	138.2	23858	69
RGF 9-41-3	Barbados	*M. annularis*	132.87	141.6	25645	40
RGF 9-41-6	Barbados	*M. annularis*	133.02	141.8	25743	61
RGF9-41-8	Barbados	*M. annularis*	133.28	142.0	25639	45
RGF 9-41-9	Barbados	*M. annularis*	133.41	142.2	25741	53
RGF 9-41-10	Barbados	*M. annularis*	133.48	142.3	25866	53
RGF 9-41-11	Barbados	*M. annularis*	133.23	142.0	25622	63
RGF 9-41-13	Barbados	*M. annularis*	133.44	142.3	26044	40
RGF 13-1-11	Barbados	*M. annularis*	95.52	100.5	14563	65
RGF 15-1-2	Barbados	*M. annularis*	81.29	85.4	11988	61
RGF 15-2-4	Barbados	*M. annularis*	83.27	87.5	12533	25
RGF 15-3-6	Barbados	*M. annularis*	85.24	89.6	12783	65
RGF 15-13-4	Barbados	*M. annularis*	104.81	111.5	19770	31
RGF 15-14-3	Barbados	*M. annularis*	106.07	112.7	19483	27
RGF 15-14-4	Barbados	*M. annularis*	106.16	112.9	19638	25
RGF 15-14-5	Barbados	*M. annularis*	106.34	113.0	19650	110
RGF 15-15-8	Barbados	*M. annularis*	108	114.8	19913	34
RGF 15-17-3	Barbados	*M. annularis*	111.05	118.1	20575	31
RGF 15-19-3	Barbados	*M. annularis*	112.25	119.3	20632	31
RGF 7-4-2	Barbados	*P. asteroides*	17.82	20.3	7376	17
RGF 9-3-5	Barbados	*P. asteroides*	81.68	86.1	12937	33
RGF 9-3-6	Barbados	*P. asteroides*	81.75	86.1	12873	24
RGF 9-32-4	Barbados	*P. asteroides*	119.77	126.7	20339	79
RGF 9-34-7	Barbados	*P. asteroides*	124.14	131.5	21714	41
RGF 9-34-8	Barbados	*P. asteroides*	124.39	131.8	21802	41
RGF 9-34-10	Barbados	*P. asteroides*	124.59	132.0	21858	41
RGF 9-35-2	Barbados	*P. asteroides*	125.27	132.8	21966	39
RGF 9-39-4	Barbados	*Diploria*	130.15	138.6	24883	55
RGF 9-39-5A	Barbados	*Diploria*	130.45	138.8	24579	41
RGF 9-40-3	Barbados	*Diploria*	132.01	140.6	25265	225
RGF 9-40-4	Barbados	*Diploria*	132.13	140.7	25045	30
RGF 9-43-3	Barbados	*Diploria*	139.77	150.5	31366	56
RGF 15-1-6	Barbados	*Diploria* spp.	81.94	86.2	12411	69
RGF 15-13-6	Barbados	*Diploria* sp	105.05	111.7	19434	30
RGF 15-15-3	Barbados	*Diploria* sp	107.5	114.2	19595	44
RGF 15-15-5	Barbados	*Diploria* sp	107.65	114.3	19627	34
RGF 16-6-2	Barbados	*A. cervicornis*	48.37	52.0	10527	46

converted the original U/Th age measurements to calendar years before present (see Table 1). For present purposes we will distinguish the sea-level index points provided by four different species of coral, respectively, *Acropora palmata* (Ap), *Montastrea annularis* (Ma), *P. asteroides* (Pa), and *Diploria* (Di). The most important index points are provided by the Ap measurements since the Ap facies, i.e. the reef zone numerically dominated by the reef crest species Ap, is restricted to a water depth within 5 m of sea level in the modern ecology (Fairbanks, 1989, as shown by

the short error bars attached to them in Fig. 2). Observations of isolated Ap colonies or storm-displaced specimens deeper than 5 m have been reported but to our knowledge Ap specimens collected from the Ap facies can be reliably assigned to 5 m or shallower water depths. However, the data derived from *M. annularis*, indicated by error bars of intermediate length, are actually of considerable value as well, as we will demonstrate. Since the living depths of the other species are not adequately restricted (long error bars) they provide only a lower limit upon RSL
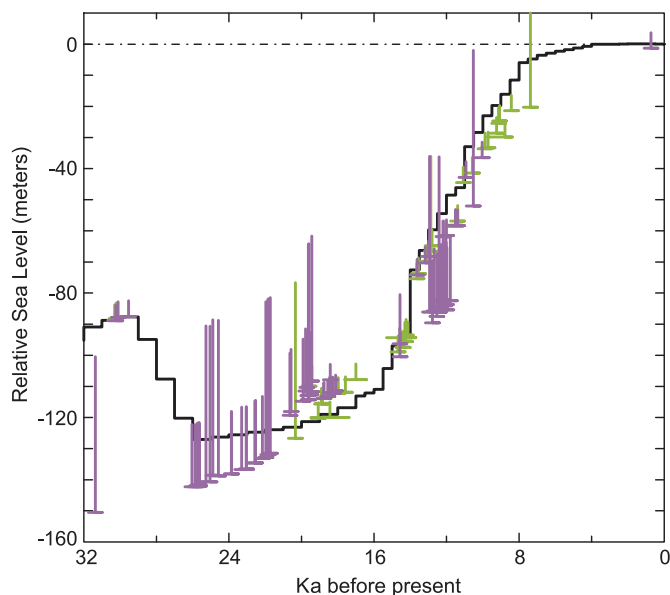
Fig. 2. The extended set of relative sea levels (RSL) observations from Barbados with individual data points show as meters below present sea level. Old data are shown in green, new data being discussed in this paper for the first time are denoted by the purple symbols. For each data point the horizontal bar denotes the depth (corrected for a rate of vertical tectonic uplift of $0.34 \, \mathrm{mm \, yr}^{-1}$) from which the sample was actually recovered. The Th/U age uncertainties are close to the thickness of the vertical lines and are therefore not plotted (see Table 1 for 1 sigma error estimates). The length of the vertical error bar denotes the range with respect to sea level within which the corresponding species of coral could be found. The shortest vertical error bars (5 m) correspond to the species Acropora Palmata, the intermediate length error bars (20 m) correspond to the species Monasterea annularis, and the error bars of greatest length to either Asteroides or Diploria. Also shown on this figure is the eustatic sea-level curve for the version of the ICE-5G (VM2) model (denoted 5GX) in which LGM has been assumed to have occurred at 26 ka rather than the conventional age of 21 ka.

history at this location. Also shown in Fig. 2 is the eustatic sea-level curve for a slight variant on the newly constructed ICE-5G (VM2) model (Peltier, 2004) of the deglaciation of the continents that will be employed as basis for discussion in what follows. In this extended version of ICE-5G (VM2), LGM has been assumed to occur at 26 ka rather than the conventional age of 21 ka, with the eustatic level being approximately 4 m lower at the earlier time. Between 21 and 15 ka the original ICE-5G (VM2) model has also been modified by assuming that deglaciation proceeded more slowly in this interval, a modification suggested by the data from the distant Sunda Shelf to be discussed further in what follows. It will be clear by inspection that the global eustatic curve for the new model of global deglaciation, fits the observed RSL history at Barbados very accurately as did the eustatic curve of the ICE-4G (VM2) precursor to this new model (Peltier, 2002a,b,c).

There are several features of the expanded Barbados data set that will be important in the ensuing discussion. Firstly, there is an crucial new set of Ap- and Ma- based measurements in the age range between 19,000 and 21,000

calendar years ago (see Table 1 for precise age–depth combinations), which suffice to rule out the existence of the additional meltwater pulse that has been hypothesized (Yokoyama et al., 2000) to have occurred at 19 ka in the earliest stage of the deglaciation process. These new data rule out the occurrence of any such sharp change of eustatic sea-level back to the conventionally assumed LGM age of 21 ka. Secondly, there is the intriguing set of RSL indicators based upon Ma samples that suggest that sea level must have been lower at approximately 26,000 years before present than at the conventionally assumed 21 ka age of LGM.

Inspection of the representation of the Ma samples in Fig. 2 reveals that the "intermediate" error range ascribed to them is 20 m. This constraint is actually rather precise and is based upon the fact that the coral Ma undergoes a sharp transition of shape in water depth greater than 18 m, from a columnar or hemispherical form at shallower depth (surface to approximately 18 m), to a flattened form at depths greater than 20 m (Land et al., 1975; Weber et al., 1976; Fairbanks and Dodge, 1979). Analysis based upon the application of X-radiography to the Ma samples in the Barbados data set establishes that all samples have the shallow water form. Thus the 20 m plausible range of sea level attached to the Ma samples is shown in Fig. 2. Also clear by inspection of these data points in Fig. 2 (and Table 1) is that this species of coral may exist either at the bottom of its range or at the top. For example, although most of the Ma samples of Younger Dryas age near 12 ka were found approximately 20 m below the depth of the Ap samples of the same age, those of age near 20 ka were found at the same level as the Ap samples. Ma is commonly found in abundance in the Acropora palmate reef facies. There is clearly an issue therefore as to how the Ma samples of age greater than 21 ka may be employed to constrain eustatic sea level. The eustatic sea-level curve of the extended version of the ICE-5G (VM2) model is one that favors the shallower portion of the range allowed by the observed shape of these coral samples, however we do not claim that the coral depth habitat range confirms the validity of this model characteristic. Furthermore, it is clear that the shallowest plausible depth for the oldest of the Ma samples at 26 ka is deeper than the Ap samples of age near 21 ka. This implies that the lowest stand of the sea could have occurred significantly earlier than 21 ka and therefore that the LGM interval could have lasted between 5000 and 7000 years (see also Lambeck et al., 2002).

The final feature of the expanded Barbados data set that will prove crucial to our interpretation of the LGM eustatic low stand of the sea is the series of Ap samples of age near 30 ka that have been recovered from a depth near 90 m (see Table 1). If actual relative sea level at the 26 ka age of the oldest Ma sample were best approximated by the deepest portion of the Ma range, then over the same 4 ka interval of time eustatic sea level would have had to fall by 50 m. For the extended version of the ICE-5G (VM2) model whose eustatic curve is shown in Fig. 2, the net fall over

this interval of time is a significantly lower value near 30 m. In order to accurately constrain the LGM eustatic level, if this is older than 21 ka, we are therefore obliged to determine where in the allowed Ma range Barbados sea-level actually existed in the period between 21 and 26 ka. Theory will prove helpful in this as will recently published results concerning the evolution of the Laurentide Ice Sheet.

2. The theory of Postglacial RSL history and the impacts of earth rotation and coastline migration

The origins of the modern theory of postglacial sea-level change are to be found in a series of papers that appeared almost 30 years ago (Peltier, 1974; Peltier and Andrews, 1976; Farrell and Clark, 1976; Peltier, 1976; Clark et al., 1978, Peltier et al., 1978). This theory has been considerably embellished since that time and was recently reviewed in Peltier (1998a,b). Its prediction of RSL history at a particular point in space, $S(\theta, \lambda, t)$ say in which θ is latitude, λ is longitude and t is time, is obtained as a solution to the following integral equation:

Γ and ϕ were first presented in Peltier (1974) and Peltier and Andrrews (1976) respectively. The further terms in (1), T and G^T, respectively, denote the perturbation to the centrifugal potential due to the alteration of the rotational state of the planet caused by the isostatic adjustment of its shape and internal mass distribution, and the Green function for the separation between the surface of the solid Earth and the equipotential surface of the sea that is induced by this applied variation of potential. The required theory for the change in rotation due to the glacial isostatic adjustment (GIA) process was first presented in Peltier (1982) and Wu and Peltier (1984) while the theory for the incorporation of the influence of rotational feedback onto sea level (at the level of first-order perturbation theory) was described in Peltier (1998a,b, 1999). Attention has recently been drawn to the importance of the influence of rotational feedback upon observed Holocene relative sea-level histories in Peltier (2002a,b,c) and Peltier (2005). There it is shown that this feedback is required to understand the anomalous high stands of the sea that are observed along the south coast of Argentinian Patagonia and that the strength of the feedback embodied in the ICE-4G(VM2)

$$S(\theta,\lambda,t) = C(\theta,\lambda,t)\left[\int_o^t dt' \iint_\Omega d\Omega' \{L(\theta',\lambda',t')G^L(\gamma,t-t') + T(\theta',\lambda',t)G^T(\gamma,t-t')\} + \frac{\Delta\Phi(t)}{g}\right]. \tag{1}$$

In this equation $C(\theta, \lambda, t)$ is the ocean function, which is by definition unity over the oceans and zero over the continents. This equation is an integral equation because the surface mass load per unit area, L, has the following composite form:

$$L(\theta,\lambda,t) = \rho_I I(\theta,\lambda,t) + \rho_w S(\theta,\lambda,t), \tag{2}$$

in which ρ_I and ρ_w are the densities of continental ice and ocean water, respectively, and $I(\theta, \lambda, t)$ is the time- and space-dependent thickness of ice on the continents. It is because S appears both on the left-hand side of (1) and also as a component of the integrand of the triple convolution integral on the right-hand side, that the equation is an integral equation. The remaining terms in Eq. (1) include $G^L(\gamma, t)$, which is the Green function for separation between the surface of the assumed spherically symmetric Maxwell viscoelastic model of the solid Earth, and the equipotential surface of the sea (γ is the angular separation between source point and field point), which has the form

$$G^L(\gamma,t) = \frac{\phi(\gamma,t)}{g} - \Gamma(\gamma,t), \tag{3}$$

in which $\phi(\gamma, t)$ is the perturbation of the gravitational potential and $\Gamma(\gamma, t)$ the perturbation of the local radius of the solid Earth that are induced by a point mass load that is applied to the surface at $t = 0$ and instantaneously removed. The mathematical methods required to compute

and ICE-5G(VM2) models of the GIA process leads to a correct prediction of the high stands documented in Rostami et al., (2000).

The final term in (1), $\Delta\Phi(t)/g$, was first discussed in Farrell and Clark (1976) using the mathematical solution for $G^L(\gamma, t)$ appropriate for a particular linearly visco-elastic Maxwell model of the Earth derivative of the work presented in Peltier (1974) and Peltier and Andrews (1976). This term is determined based upon the requirement that the GIA process conserve mass, i.e. that the mass of ice that is melted from the continents equals the mass of water that enters the ocean basins. The first solutions to Eq. (1) were presented in Clark et al., (1978) and Peltier et al., (1978) together with comparisons of these theoretical predictions to observations of relative sea-level change through the Holocene epoch (most recent 10,000 years) of Earth history, observations for which chronological control was provided by ^{14}C dating of the pertinent sea-level index points. Even these earliest inter-comparisons of theory and observations demonstrated that the theory appeared to capture all of the most essential spatial variability contained in Holocene observations. Especially important was the fact that the gravitationally self-consistent nature of the theory led to a direct prediction of the occurrence of the mid-Holocene high stands of the sea that had been observed to be a characteristic of relative sea-level histories at all oceanic islands in the equatorial Pacific Ocean.

Although recent research has shown that even rather subtle characteristics of Holocene records from particular geographical regions, such as that due to the influence of rotational feedback (Peltier 2002a,b,c, 2005), are extremely well explained by the complete theory, a current focus of work in this field has come to be upon the issue previously discussed as to the implications of theory for the amount of ice that must have been resident upon the continents at LGM. Our interest in the present paper is not only upon this important property of the glaciation–deglaciation process but also upon the longevity of the LGM interval of time.

The methodology that we will employ for the theoretical analyses to be discussed herein is a further refinement of that described recently in Peltier (2005), a method for the solution of Eq. (1) that is especially well suited for computation of sea-level histories when a complete cycle of glaciation and deglaciation is employed for continental ice sheet history, even in circumstances in which the land–sea interaction is as complex as that described in Tarasov and Peltier (2004). This methodology begins by invoking the globally accurate algorithm for the computation of the time dependence of the ocean function $C(\theta, \lambda, t)$ that was first presented in Peltier (1994, 1996) and this remains central to the refined method for the solution of (1) to be employed for present purposes. We begin by first re-writing (1) in the schematic form, following the discussion in Peltier (2005), as

$$S(\theta, \lambda, t) = V(\theta, \lambda, t) + D(t) \qquad (4)$$

from which the explicit appearance of the multiplicative factor C has been eliminated because the field S is defined everywhere over the surface of the planet, even where there is no ocean. The function $S(\theta, \lambda, t)$ of latitude, longitiude and time is simply the perturbation of the height of the geoide (the surface of constant gravitational potential that is coincident with the surface of the sea where ocean exists) relative to the surface of the solid Earth. Now Eq. (4) may be solved discretely in time using the iterative procedure described in detail in Peltier (1998a,b) in which the full influence of rotational feedback on sea-level history is incorporated. Suppose that we consider the change in sea level between the $n-1$st time step and the nth time step. If $C_n = C_{n-1}$, then the change in the thickness of the water load at a given point on the surface, and thus relative sea level, would simply be $(S_n - S_{n-1})\, C_n$. However, if $C_n \neq C_{n-1}$ then the change in water load will not be accurately estimated by this expression at those locations where C_n differs from C_{n-1} because of coastline migration.

In fact there are several sources of error that arise due to the temporal evolution of C, sources that act within the interior of the zone where initially glaciated regions later become inundated by the sea (or vice versa), and a source in those locations outside the zones of glaciation in which, for example, initially exposed continental shelf is being inundated by the sea due to the melting of continental ice. Both of these sources of error were explicitly recognized in Peltier (1998a,b). In previous work on the influence of

time-dependent ocean function, these two regions were treated separately. In particular, the interior region was addressed by accounting for the action of "implicit ice" (Peltier, 1998a,b) and the exterior region has been dealt with by recognizing the influence of a "broad shelf effect" (Peltier and Drummond, 2002).

In the algorithm that will be employed for the analysis of this problem to be reported herein, a further enhancement of that reported in Peltier (2005), the interior and exterior regions in which C varies are treated simply by storing knowledge of the increment in sea level S_{n-1} obtained in the previous time-step in the iterative solution of Eq. (1) as well as the form of the ocean function, C_{n-1}, and paleotopography T_{n-1} that obtained at the same time. We then compute the actual sea-level change in the regions of changing C, using expressions that respect the volume of the ocean lost or gained between the evolving paleotopography and the equipotential surface of the sea.

We begin the development of the enhanced computational scheme by considering the imposition of the mass conservation constraint for the nth time step in the iterative solution of Eq. (1). This constraint is expressed by the term $D(t)$. Suppose that the mass of ice melted in the nth time step, ΔM_n^I say, is simply:

$$\Delta M_n^I = \rho_I \langle \Delta I_n \rangle, \qquad (5)$$

where ρ_I is the density of ice, ΔI_n is the longitude and latitude dependent change of the thickness at the nth time step and $\langle \ \rangle$ indicates integration over the region of the continents in which the ice load is changing. This change in the continental ice load will give rise to a change in water load that we may denote by ΔW_n to which there will exist a number of contributions. The distinct expressions for four such contributions combine to produce the following mathematical expression for this quantity:

$$\Delta W_n = \rho_w \langle \Delta S_n \rangle |\text{Area1} + \rho_w \langle (-T_n) \rangle |\text{Area2} \\ - \rho_w \langle (-T_{n-1}) \rangle \big| \text{Area3} + \rho_w \langle (h_{n-1} - h_n) \rangle |\text{Area4} \qquad (6)$$

in which the first term is to be integrated over Area1 which consists of those areas that were ocean at time step $n-1$ and are still ocean at time step n. Similarly the second term is integrated over Area2 which is the area of new ocean, the third term over Area3 which is the area of new land and the fourth term is integrated over Area4 that consists of areas that were and are still ocean but which also contain grounded ice. In these expressions T_n is the paleo-topography at the nth time step calculated as in Peltier (1994) and h_n is the thickness of the grounded ice at the nth time step. By employing the correct mathematical expressions for the different areas of integration for each of the above four terms, the final form for the change in water load becomes

$$\Delta W_n = \rho_w \langle \Delta S_n C_n C_{n-1} \rangle + \rho_w \langle (-T_n) C_n (C_n - C_{n-1}) \rangle \\ - \rho_w \langle (-T_{n-1}) C_{n-1} (C_{n-1} - C_n) \rangle - \rho_w \langle \Delta h_n C_n C_{n-1} \rangle. \qquad (7)$$

The complete expression for the paleotopography at the nth timestep in the iterative solution of (1) is then

$$T_n = T_{n-1} + \Delta h_n - \Delta S_n. \tag{8}$$

This may be employed to replace the function T_n in the second term of Eq. (6). To complete the definition of the expression for the incremental change in the water load we must also introduce the idea of a "runoff function" that we will denote by "R" such that

$$R_n = (-T_n)C_{n-1}(C_{n-1} - C_n), \tag{9}$$

a function that is positive on "new" land but is otherwise zero. This is introduced to allow us to capture the impact upon the mass conservation term when previously water covered land is replaced by ice-covered land (e.g. during the glaciation phase of the ice age cycle when previously water covered Hudson Bay becomes covered by ice). Incorporating these further considerations into (6), we obtain the further refined expression:

$$\begin{aligned}
\Delta W_n &= \rho_{\mathrm{w}}\langle \Delta S_n C_n C_{n-1}\rangle - \rho_{\mathrm{w}}\langle \Delta h_n C_n C_{n-1}\rangle \\
&\quad + \rho_{\mathrm{w}}\langle \Delta S_n C_n (C_n - C_{n-1})\rangle - \rho_{\mathrm{w}}\langle \Delta h_n C_n (C_n - C_{n-1})\rangle \\
&\quad + \rho_{\mathrm{w}}\langle(-T_{n-1})C_n(C_n - C_{n-1})\rangle - \rho_{\mathrm{w}}\langle R_n\rangle
\end{aligned} \tag{10a}$$

$$\begin{aligned}
&= \rho_{\mathrm{w}}\langle \Delta S_n C_n C_n\rangle - \rho_{\mathrm{w}}\langle \Delta h_n C_n C_n\rangle \\
&\quad + \rho_{\mathrm{w}}\langle(-T_{n-1})C_n(C_n - C_{n-1})\rangle - \rho_{\mathrm{w}}\langle R_n\rangle
\end{aligned} \tag{10b}$$

$$\begin{aligned}
&= \rho_{\mathrm{w}}\langle \Delta S_n C_n\rangle - \rho_{\mathrm{w}}\langle \Delta h_n C_n\rangle \\
&\quad + \rho_{\mathrm{w}}\langle(-T_{n-1})C_n(C_n - C_{n-1})\rangle - \rho_{\mathrm{w}}\langle R_n\rangle.
\end{aligned} \tag{10c}$$

If we further define $\Delta A_n = \Delta h_n C_n$ and $\Delta B_n = (+T_{n-1})C_n (C_n - C_{n-1})$, the former being positive for increasing glaciation and negative for deglaciation, and the latter being positive on new ocean but otherwise zero (previously described as the "broad shelf effect" in Peltier and Drummond (2002), then we may write the expression for the conservation of mass at the nth time step as

$$\rho_{\mathrm{w}}\langle \Delta S_n C_n\rangle = \rho_I \langle I_n\rangle + \rho_{\mathrm{w}}\langle \Delta A_n + \Delta B_n + \Delta R_n\rangle. \tag{11}$$

Implementation of this result in Eq. (4) then delivers the expression

$$\begin{aligned}
&\langle(V_n - V_{n-1})C_n\rangle + (D_n - D_{n-1})C_n \\
&= \frac{\rho_I}{\rho_{\mathrm{w}}}\langle I_n\rangle + \langle \Delta A_n + \Delta B_n + \Delta R_n\rangle
\end{aligned} \tag{12}$$

so that:

$$\begin{aligned}
&D_n - D_{n-1} \\
&= \frac{\rho_I}{\rho_{\mathrm{w}}}\frac{\langle \Delta I_n\rangle}{\langle C_n\rangle} - \frac{\langle(V_n - V_{n-1})C_n\rangle}{\langle C_n\rangle} + \frac{\langle \Delta A_n + \Delta B_n + \Delta R_n\rangle}{\langle C_n\rangle},
\end{aligned} \tag{13}$$

which is the expression for the increment in the mass conservation term that must be added to the right-hand side of Eq. (1) between the nth and preceding time steps. This is a completely general result and, when comparing it to the interim result presented in Peltier (2005), will be seen to involve a slight extension, one that will nevertheless be

important in the future as the theory is employed to assimilate complex models of the glacial cycle such as those delivered by climate forced models of continental ice dynamics (see e.g. Tarasov and Peltier, 2004 for an example of the product of such analyses). The iterative method that is employed to solve (1), say at the nth time step, begins with a first approximation for the space dependent increment ΔS_n as

$$\Delta S_n = \frac{\rho_I}{\rho_{\mathrm{w}}}\langle \Delta I_n\rangle\frac{C_n}{\langle C_n\rangle} + \langle \Delta A_n + \Delta B_n + \Delta R_n\rangle\frac{C_n}{\langle C_n\rangle}. \tag{14}$$

This is then employed to calculate the change in water load which delivers a value for V_n which in turn implies from (12) a result for $D_n - D_{n-1}$ and this in turn gives a new result for $\Delta S_n = (V_n - V_{n-1}) + (D_n - D_{n-1})$. The sequence of steps in the iteration process is continued until convergence is achieved and thus leads to a final form for the space dependent field $S_n = V_n + D_n$ at the nth time step.

3. Eustatic sea-level rise across the glacial–interglacial transition

In order to demonstrate the implications of this algorithm for understanding the constraint upon the postglacial eustatic rise provided by available observations, we will employ the recently published, and geologically and geophysically well-constrained model of the deglaciation of the continents denoted ICE-5G (VM2) and described at length in Peltier (2004). To develop a full glacial cycle of surface ice loading and unloading we employ the Martinsen et al. (1987) SPECMAP record of δ^{18}O history to constrain the evolution of the volume of land ice from the last (Eemian) interglacial up to LGM, assuming that during glaciation the area of the continents covered by ice remains equal to the LGM coverage and that ice thickness simply rises synchronously with δ^{18}O so as to achieve the thickness distribution of the ICE-5G (VM2) model by LGM.

Fig. 3 shows the fit of the predictions of the ICE-5G (VM2) model to observed Holocene records of postglacial RSL history at 8 different geographical locations, with the sites of the individual RSL observations shown superimposed upon a global map of the model predicted present day rate of sea-level rise. The sources of the Holocene RSL data plotted in each of the eight inter-comparisons are provided in the list of references at the end of the paper. Inspection of the comparisons between theoretically predicted and geologically inferred RSL histories will demonstrate that the model reasonably reconciles the observations at all locations over the Holocene period. It should be understood that the data at ice-sheet centered sites such as SE Hudson Bay in Canada and Angerman River in Sweden have been employed to tune the model for both ice sheet thickness and the radial profile of mantle viscosity (e.g. see Peltier, 1982).

Of greatest interest from the perspective of the present paper, however, are the predictions that are made by the new model of the LGM depression of RSL given the
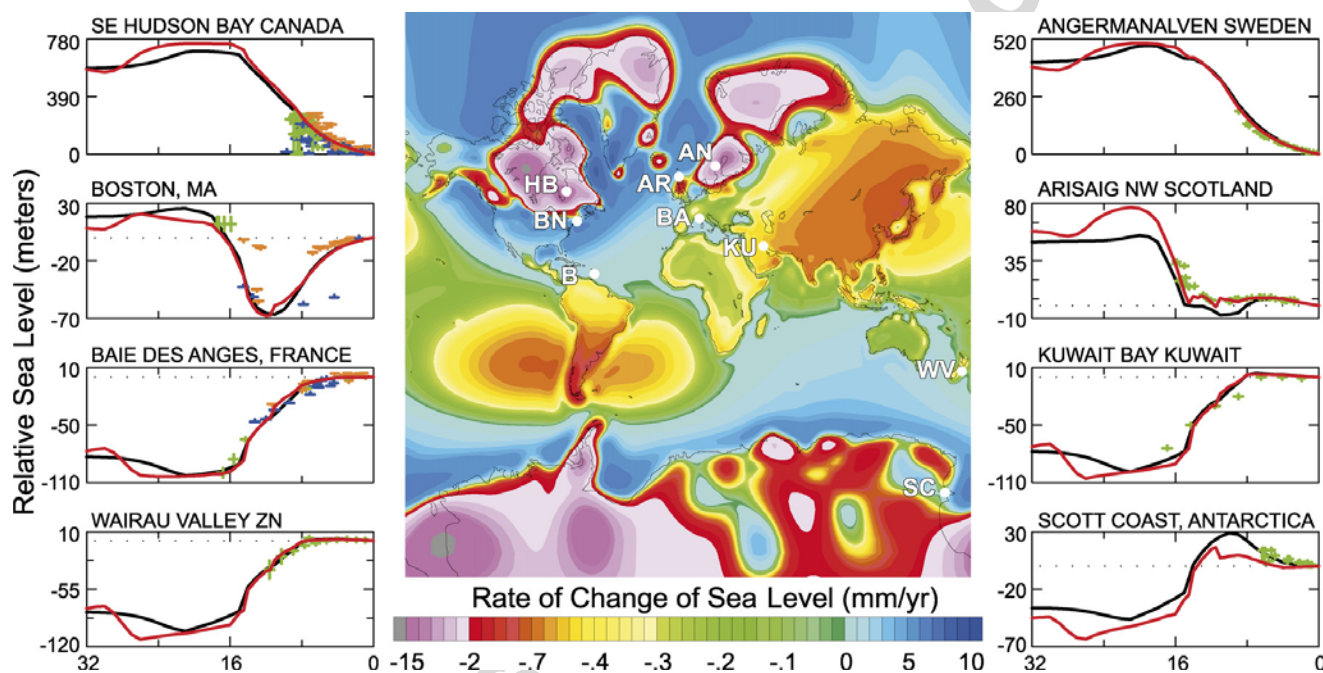
Fig. 3. The locations of eight sites from which high-quality Holocene records of RSL history are available are shown in the center frame superimposed upon the ICE-5GX (VM2) model prediction of the present day rate of change of relative sea level that would be observed as a secular rate of change on a tide gauge recording of sufficient duration. In the eight additional frames of the figure intercomparisons are shown between the theoretically predicted and geologically inferred Holocene RSL histories at each of these locations for both the original (black curves) and the extended (red curves) versions of the model. The sources of the data employed for these inter-comparisons are as follows: HB (Peltier, 1998b), BN (Kaye and Barghoorn, 1964), BA (Dubar and Anthony, 1995), WV (Pickerill, 1976), AN (Cato, 1992), AR (Shennan et al., 1993), KU (Al-Asfour, 1982), SC (Hall and Denton, 1999).

eustatic, continental ice-equivalent, sea-level variation that the model includes. The eustatic ice-equivalent sea-level history of the extended version the ICE-5G (VM2) model, from 32,000 calendar years ago until the present, is shown as the piecewise discontinuous curve plotted together with the Barbados RSL data in Fig. 2. Inspection will demonstrate two important facts; firstly, the ice-equivalent eustatic sea-level curve of the model in which LGM is assumed to have occurred at 26,000 years before present, is characterized by a net increase of 122.7 m (when evaluated in terms of the fixed modern surface area of the oceans). It is important to note that this eustatic curve actually provides a rather good fit to the Barbados record itself. Since this location on Earth's surface is one at which local sea-level history is expected to provide a very good approximation to global, ice-equivalent, eustatic sea-level history (Peltier, 2002a,b,c), an acceptable model of deglaciation must have this property. The reason why the RSL record from Barbados provides such a good approximation to postglacial eustatic sea-level history will be clear from the map of the modern rate of RSL rise shown in Fig. 3 in which Barbados is seen to be located on the trailing edge of the proglacial forebulge within which sea level is continuing to rise due to the influence of forebulge collapse. The Island of Barbados therefore acts essentially as a metre stick attached to the sea floor on which sea level is not influenced significantly by the deformation of the solid earth. Secondly, it is notable that, although the ICE-5G(VM2) model embodies highly significant differences in the spatial distribution of continental ice-thickness (as discussed in Peltier, 2004), the net LGM eustatic depression is quite close to this characteristic of the ICE-4G (VM2) precursor model (Peltier 1994, 1996), which was 117.8 m when implicit ice of both types I and II was taken into account and isostatic equilibrium was assumed at LGM. In fact the eustatic depression of sea level at LGM characteristic of the version of the original version of ICE-5G (VM2) described in Peltier (2004), which assumes the conventional age of LGM of 21 ka, is 118.7 m, essentially identical to that of the previous ICE-4G (VM2) model.

In Fig. 4 we show the predictions of the history of postglacial RSL at Barbados using as input to Eq. (1) the new ICE-5G (VM2) model. Results are shown for two different variants on the calculation and for two slightly different versions of the model. The first of these versions is ICE-5G (VM2) *senso stricto*, in which LGM is assumed to have occurred at 21,000 calendar years before present. Results are shown for two variants on this prediction, one which excludes and one which includes the influence of rotational feedback and intercomparison will show that the influence of this feedback at Barbados is small and such as to slightly reduce the predicted RSL depression at LGM from that produced by theory when this influence is excluded. The main result which follows from this set of model-data intercomparisons is that the ICE-5G (VM2) model, whose eustatic RSL depression at LGM is 118.7 m,
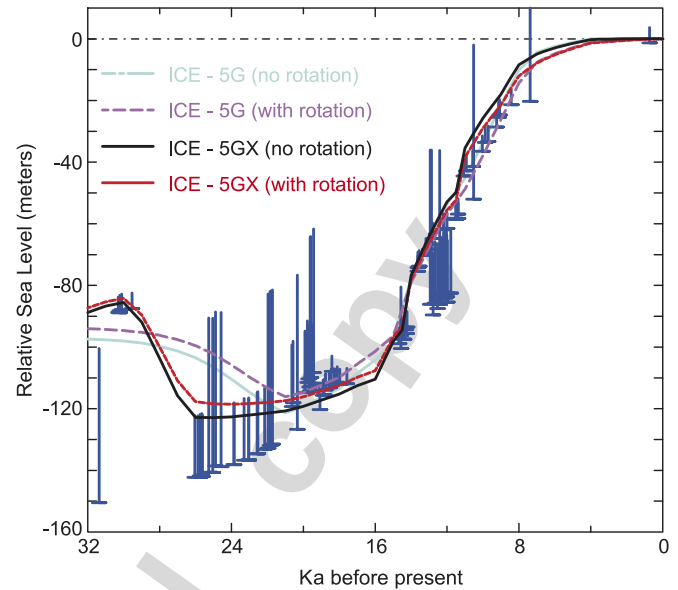

Fig. 4. Observations of RSL index points at Barbados compared to the predictions of the theory of postglacial relative sea-level change embodied in Eq. (1) of the paper. Theoretical predictions are shown for both the original ICE-5G model (31) and for the extended version of this model in which LGM is assumed to have occurred at 26 ka (denoted 5GX). For both of these models, which are characterized by LGM eustatic sea-level depressions of 118.7 and 122.4 m respectively, theoretical results are shown which both include and exclude the influence of rotational feedback.

fits the observations at Barbados extremely well back to the conventional LGM age of 21 ka.

Also shown in Fig. 4 are results for an equivalent pair of calculations in which the ICE-5G model of deglaciation is extended to an LGM that is assumed to have occurred 26,000 years before present. For this variant upon ICE-5G (VM2), the LGM ice-equivalent eustatic depression is 122.7 m as previously noted, the additional 4 m of ice-equivalent RSL rise having been added to the deglaciation model in order to accommodate the suggestion based upon the Ma data that RSL was slightly lower at Barbados at 26 ka than it was at 21 ka, and therefore that the usually assumed timing of LGM of 21 ka may be wrong by as much as 5 ka. At minimum, these Ma-based data are interpreted to define a 5 ka broad interval within which relative sea level may have remained almost stationary at the LGM level although they do not by themselves rule out the possibility that an abrupt change of sea level might have occurred prior to 21 ka.

It is important to note that the cluster of excellent Ap-based samples, of age near 30 ka, at an adjusted depth near 90 m, are also well fit by the extended version of the ICE-5G model, suggesting, according to this reconstruction, that approximately 30 m sea-level equivalent, or fully 25% of the mass of LGM ice, could have accumulated in less than 5,000 years prior to glacial maximum. That this rapid increase of global ice volume was most probably entirely due to a rapid westward expansion of the Laurentide Ice

Sheet (LIS) is strongly suggested by recently published a priori reconstructions of the LIS (Tarasov and Peltier, 2004), and is more directly demanded by the observed geomorphology of the Keewatin sector of the Canadian Shield (Dyke et al., 2002).

Now it might be argued that the ICE-5G (VM2) model has in fact been tuned to enable it to fit the Barbados record and that this undercuts the importance of the high quality of the fit to these data that the model has delivered. In fact this is true to a certain degree. Although the mass distribution of each of the northern hemisphere ice sheets is constrained primarily by local observations of RSL history and a variety of geomorphological and modern geodetic constraints as discussed in Peltier (2002a,b,c), and not by Barbados data, there is very little such information available on the basis of which we may constrain the history of Antarctic ice thickness changes and this is an important contribution to the net eustatic rise of RSL. As discussed in Peltier (2004), the ICE-5G model is identical to the ICE-4G model insofar as its Antarctic component is concerned and embodies a net eustatic rise of 16.8 m from this region. This is insignificantly higher than the approximately 14 m suggested on the basis of a priori glaciological reconstructions of the Antarctic Ice Sheet alone (Denton and Hughes, 2002; Huybrechts, 2002). Furthermore, although the timing assumed for the removal of this component of the LGM excess ice load was originally constrained so as to eliminate the misfit to far field RSL records that otherwise obtained (e.g. see Peltier, 1998a,b), strong support for the assumed late deglaciation of Antarctica inferred on this basis has recently been forthcoming based upon direct exposure age dating of previously glaciated surfaces (personal communication from G.H. Denton, Domack et al., 2005).

It is therefore clear that the Barbados record does not play an overly important role in tuning the history of continental ice volume change although it is the sole basis on which the strong MWP1a event (derived primarily from Laurentia, see Peltier, 2005; Tarasov and Peltier, 2005) has been introduced into this assumed history. That the climatological basis for the appearance of this event is reasonable has been recently demonstrated in Tarasov and Peltier (2004) where an ice dynamics reconstruction of the growth and decay of Laurentide ice over the last glacial cycle has been shown to deliver a significant fraction of the dramatic MWP1a event based solely upon the physical interactions included explicitly in the formulation of the model. The delayed deglaciation embodied in ICE-5G for the Antarctic component of the model, which so well fits the available constraints, is distinctly at odds with the recent suggestion by Clark et al. (2002) that all of MWP1a could have been sourced from this region, the basis for which suggestion appears to be unsound (Peltier, 2005; see also Domack et al., 2005). This suggestion has also been strongly undermined by the locations and timing of meltwater plumes recorded by the $\delta^{18}O$ content of surface dwelling planktonic foraminifera (Fairbanks et al., 1992)

and the recent re-analysis by Seidov et al., (2006) of the expected impact of southern ocean freshening upon the strength of the Atlantic overturning circulation. Their analysis with the fully coupled GFDL atmosphere–ocean general circulation model demonstrates that the ocean only results of Weaver et al. (2003), which strongly supported the plausibility of the hypothesis of southern ocean freshening as the ultimate cause of the Bolling-Allerod warming of the northern hemisphere, are not recovered when full atmosphere–ocean coupling is allowed to determine the nature of the climate response.

It is also clearly of value to investigate whether other far field records of postglacial RSL history might exist, aside from Barbados, that could be employed to confirm or to deny the reasonableness of the ICE-5G model of planetary deglaciation with its approximately 120 m of eustatic ice-equivalent sea-level rise. For this purpose the most useful set of data is that from the Sunda Shelf of Indonesia (Hanebuth et al., 2000). Although data has also recently become available from the Vietnam Shelf (Schimanski and Stattegger, 2005) there is evidence of local differential motion that suggests it to be less useful as a sea-level constraint. The locations of the cores from which the Sunda Shelf data were derived are shown in Fig. 5, on which we also illustrate, in terms of modern topography/ bathymetry, the significant degree to which the continental shelf would have been exposed in this region at LGM when sea level was depressed by approximately 120 m. Inter-comparisons between theory and observations for the extended version of the ICE-5G model discussed in connection with Fig. 4 are shown in Fig. 5a. Clearly evident by inspection of this figure is that the Sunda Shelf record is extremely well fit by the same model that so accurately reconciles the Barbados data set. Of utmost importance is that the MWP1a event is also evident in the Sunda Shelf record where it is extremely well constrained, as the samples that delimit it are all of tropical mangrove which is an excellent sea-level marker. Since the oldest data point from the Sunda Shelf is at 21 ka, the data cannot discriminate between the original and extended versions of ICE-5G (VM2). Also evident by inspection of this figure is that the influence of rotational feedback at this site is important in enabling the model to provide such an accurate fit to the observations. In the absence of the increased depression of the predicted RSL record for LGM due to this influence, the theory would misfit the observations to a significant degree. The most important result of the Sunda Shelf comparisons, however, is that these data strongly support the interpretation of the Barbados data shown in Fig. 4 and therefore the estimate of 118.7 m (~120 m) for the LGM eustatic low stand of the sea if LGM occurred at the conventional age of 21 ka and the mapping from continental ice volume to eustatic sea-level history is produced by assuming that the surface area of the oceans remained equal to the modern area, in accord with the assumption made in inferring the glacial–interglacial variation of eustatic sea-level on the basis of Oxygen
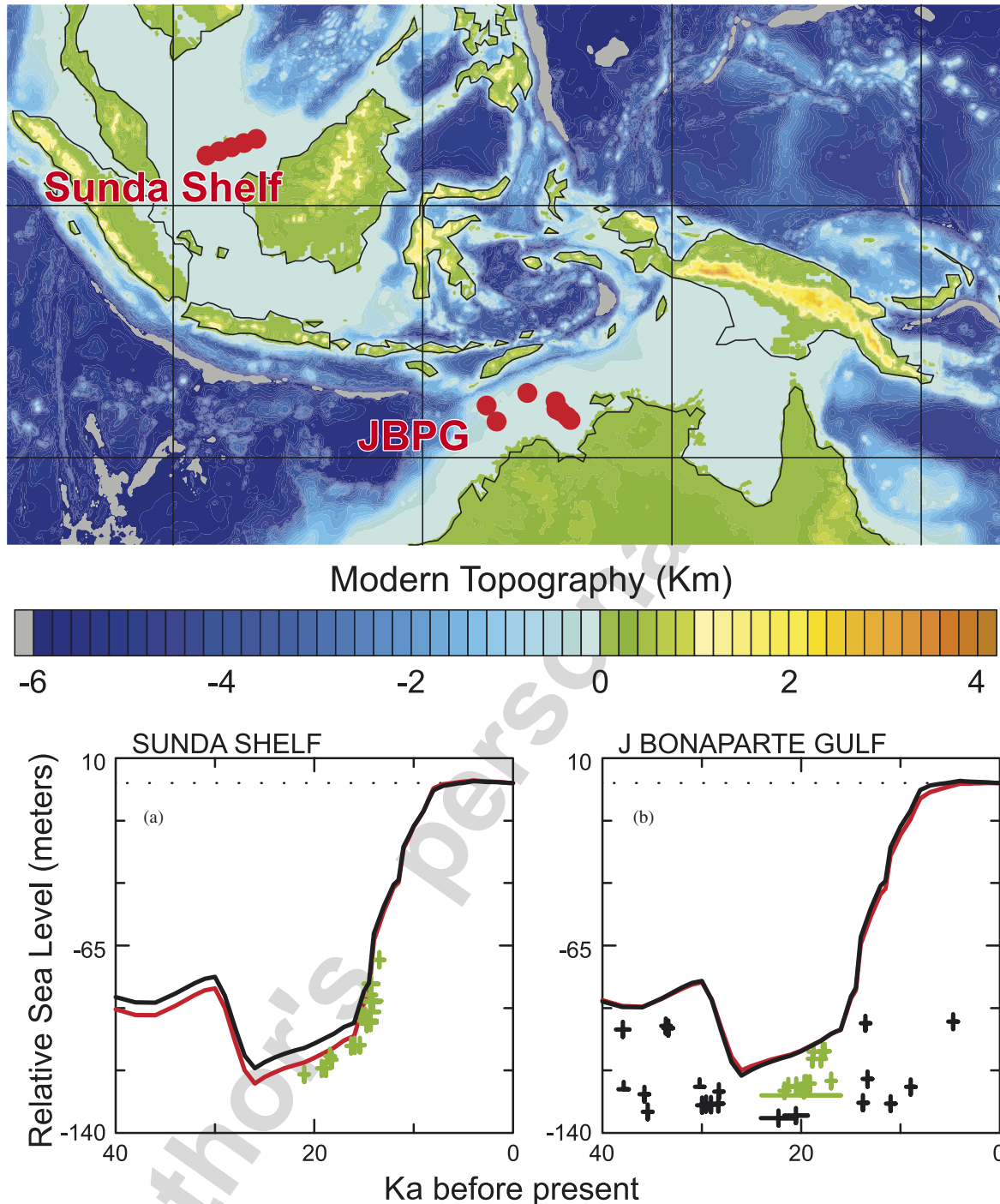
Fig. 5. Locations of the sedimentary cores employed to characterize the LGM low stand of the sea at the Sunda Shelf and J. Bonaparte Gulf locations. (a) Intercomparison of the RSL observations from the Sunda Shelf shown as green crosses (5), together with the theoretical predictions for the same suite of models employed for the analyses presented in Fig. 4. (b) Same as (a) but using the significantly less coherent set of data from the J. Bonaparte Gulf location (7). The data points shown as green in this Fig. are those invoked by the authors as basis for suggesting that a significant meltwater pulse could have occurred 19,000 years before present. Such an event is ruled out by the extended Barbados data set that we have compiled for the purpose of this paper. The data from the Sunda Shelf agree with the Barbados data in rejecting this hypothesis.

Isotope measurements from deep sea sedimentary cores (see below). Since the surface area of the oceans does diminish as one goes further back in time towards the LGM interval, however, it will be clear that if one were to

compute the average fall of sea level in such a way as to account for this time dependence in the surface area of the oceans, one would infer a greater fall of eustatic sea level to have been characteristic of LGM. This would not,

however, allow for a direct inter-comparison of the results from the model for the ice equivalent eustatic low stand of the sea with the results obtained on the basis of Oxygen Isotope analysis.

Also shown in Fig. 5b are inter-comparisons of the predictions of the model which fits both Barbados and the Sunda Shelf with a recently published record from the nearby J. Bonaparte Gulf location in northern Australia. These data were invoked in Yokoyama et al. (2000) to suggest that the eustatic low stand of the sea must have been considerably deeper than the conventional estimate of approximately 120 m. Inspection of the figure will show that the data from this site appear to be of significantly inferior quality than are those from the Sunda Shelf. The small subset of these data employed by Yokoyama et al. in their argument for a much increased LGM low stand are denoted by the colored symbols in Fig. 5b, the subset of the samples that the authors believe to provide the best constraints upon the LGM level of the sea. A possible reason as to why one might be suspicious of the utility of

these data has recently been suggested by Shennan and Milne (2003) who have drawn attention to the fact that there is no stratigraphic continuity between the measurements taken from the individual sedimentary cores (locations of which are shown in Fig. 5) that constitute the source of the data. It may be the case that there has been significant reworking of the samples from this region, rendering them unsuitable for constraining sea-level history. This possibility must remain a subject for future investigation.

The full implications of the results of these new analyses are summarized in Fig. 6 on which we have superimposed the results of three different estimates of global ice equivalent sea-level history. In the foreground of this figure we have once more placed the complete set of available data from the Barbados location upon which is the superimposed prediction of the ICE-5G(VM2) model of the global process of glacial isostatic adjustment. Also on this portion of the figure, however, we have superimposed the estimate of ice equivalent eustatic sea-level
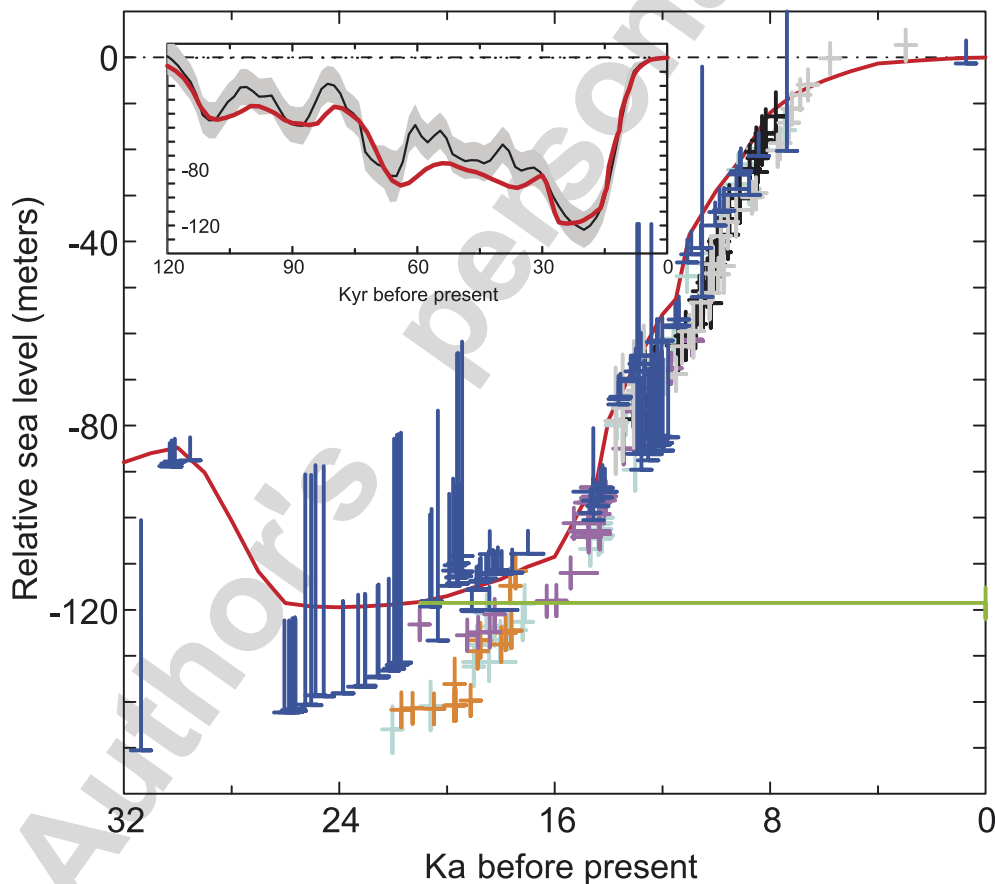

Fig. 6. Compares the eustatic ice equivalent sea-level history estimate provided by the coral-derived record from the island of Barbados shown by the blue symbols with the estimate of the same characterization of the most recent deglaciation event provided by Lambeck and Chappell (2001). The prediction of the ICE-5G(VM2) model for the Barbados location over the same range of time is denoted by the red curve. The color coding of the Lambeck and Chappell estimates, which are shown as the crosses, is as follows: cyan (Barbados), orange (Bonaparte Gulf), black (Huon Peninsula), grey (Tahiti), purple (Sunda Shelf). As discussed in the text, it will be noted that the data from both Barbados and Bonaparte Gulf are plotted 20 m below the depth from which the samples were actually recovered. Inset shows the reconstruction by Waelbroeck et al. (2002) of the complete Eemian to present ice-equivalent eustatic sea-level history based upon calibrated deep sea core derived oxygen isotopic measurements. This reconstruction is denoted by the central black curve and the surrounding error envelope is shown as stippled. The prediction of the history of sea-level change over the same period using the ICE-5G(VM2) model is again shown by the red curve.

history of Lambeck and Chappell (2001) for which the individual data contributing to the estimate are shown as color-coded crosses. It will be immediately apparent that the Lambeck and Chappell estimate of the LGM low stand of the sea is approximately 20 m deeper at 21 ka than is allowed by the Barbados data of the same age. Yet it will also be noted that the data that define the depth of their 21 ka 140 m low stand of the sea include data from the Barbados location! Since it has been demonstrated in Fig. 2, confirming the result previously presented in Peltier (2002a,b,c), that the Barbados data themselves provide a direct and accurate estimate of the depth of the globally averaged (eustatic) ice equivalent low stand of the sea, the Lambeck and Chappell result is clearly incorrect. Their reason for plotting the Barbados data ~20 m deeper than the depth at which they are actually found is that presented in Yokoyama et al. (2000). A mathematical problem in their methodology (discussed in detail in Peltier, 2002b) elicited the retraction published in Yokoyama et al. (2001). The estimate of the ice equivalent eustatic history published in Lambeck and Chappell (2001), however, has not been retracted. Yet, as will be clear on the basis of Fig. 6, it too is in conflict with the results of the analyses herein. Also of note in Fig. 6 is the fact that the Lambeck and Chappell plot of the data from J. Bonaparte Gulf has shifted these data, as well as those from the Barbados location, lower than the depth at which the samples are actually found (see Fig. 5b) by the same ~20 m. The Lambeck and Chappell (2001) estimate of the global ice equivalent eustatic curve is therefore, on this further basis, questionable at best. It does not seem plausible that this difference of interpretation could be due to a difference in the model employed for the radial variation of mantle viscosity as the majority of the difference in the LGM low stand shown on Fig. 6 is due to the postulated but apparently nonexistent 19 ka meltwater pulse.

Also shown in the inset to Fig. 6 is the independent estimate of the ice equivalent eustatic sea-level history through the entire last glacial–interglacial cycle from the end of the Eemian interglacial at 120 ka through to the present interglacial. The estimate derived by Waelbroeck et al. (2002) shown on this part of the figure and denoted by the black curve, with the surrounding stippled region defining an error envelope, has been inferred on the basis of a calibration of deep sea core derived oxygen isotopic data. In their analysis, the calibration included an attempt to carefully account for the contamination, of what is otherwise an excellent proxy for the variation of land ice volume through time, due to the variation of the temperature of the abyssal ocean. Also superimposed upon this portion of the figure and represented by the red curve is the predicted history of postglacial sea-level change at the island of Barbados through the same interval of time. It will be observed that the Waelbroeck et al. estimate of the ice-equivalent sea-level history and the Barbados history according to the ICE-5G(VM2) model are in very close accord. In particular they agree as to the best estimate of

the LGM eustatic low stand of the sea as being ~120 m. Since the full global ice thickness vs time history for the ICE-5G model is now publically available (http://www.sbl.statkart.no/projects/pgs/ice_models/Peltier_ICE-5G_v1.2/) it will be possible for the interested reader to verify the accuracy of these results for her/himself.

4. Summary

The fact that the newly constructed solutions to Eq. (1) that employ the refined technique described in Peltier (2005) for computation of RSL history over the course of a full glacial–interglacial cycle (as further refined in the present paper), simultaneously fit the LGM sea-level low-stand observations from Barbados and the Sunda Shelf is important. The fit at Barbados is especially important in itself as the record from this location (Fairbanks, 1989; Bard et al., 1990) has been shown to provide a very good direct estimate of global eustatic RSL history (Peltier, 2002a,b,c). Thus the observed ~120 m depression of RSL at Barbados IS the LGM ice-equivalent eustatic depression IF the LGM is taken to be defined by the conventional 21 ka age and IF one computes the ice volume equivalent depth of the low stand on the basis of the assumption that the surface area of the oceans at LGM remained the same as at present. On the basis of the multiple Ma-derived data now available in the range 21–26 ka, we may however conclude that sea level may have been somewhat lower prior to 21 ka, but by no more than approximately 5 m. This suggests that the Last Glacial Maximum interval may have been between 5000 and 7000 years long. Between 26 and 30 ka the Ap samples of the latter age require RSL to have been higher by approximately 30 m than the assumed LGM low stand. The fact that recent observationally constrained reconstructions of the evolution of the LIS by Tarasov and Peltier (2004) have predicted precisely this same 30 m fall of sea level as being due to the growth of the Keewatin Dome of the LIS provides further confirmation of our interpretation of the depth of the maximum eustatic depression that could have been characteristic of LGM.

The fit at the Sunda Shelf is also extremely important, however, as it shows that, if proper account is taken of the impact of coastline migration (an effect that does not influence the model predictions for Barbados) and rotational feedback, then the model that fits the Barbados data also reconciles the observations at a site "half-a-world" away. In particular, models for which the eustatic low stand is between 118.7 and 122.7 m both fit the low stand recorded at this site. This fact establishes that the physical assumptions upon which the theory of postglacial sea-level change has been developed are sound and that the constraint that the theory provides upon the LGM depression of eustatic sea-level is robust. That this constraint agrees extremely well with that derived on the basis of Oxygen Isotope analysis (Waelbroeck et al., 2002) is clearly important.

A further significant conclusion that follows from our analysis concerns the issue as to the extent to which Antarctica was involved in the transition from glacial to interglacial conditions. In Lambeck and Chappell (2001) it was suggested that insufficient land ice existed in the northern hemisphere at LGM to explain the net eustatic rise from LGM to present and that this required a much larger contribution from Antarctica than is contained, for example, in the ICE-5G (VM2) model. This argument is not supported by the analyses reported herein. Although the ICE-5G (VM2) model has significantly reduced ice cover over both Greenland and Eurasia, as discussed in Peltier (2004), the increased mass of continental ice required over North America to the west of Hudson Bay in order to fit the available geodetic constraints discussed in Peltier (2002a,b,c), more than makes up for the diminution of mass to the east. Our demonstration of the robustness of the constraint on net ice volume provided by the net eustatic rise of ∼120 m implies that Antarctica could have lost no more mass than that suggested on the basis of a priori glaciological reconstructions. Mass loss from Antarctica therefore could not have been a significant contributor to MWP1a, especially since the mass that was lost primarily occurred following the Younger-Dryas event, and coincided in its onset with the occurrence of MWP1b that is now also much better resolved in the extended Barbados data set than was previously the case. The fact that MWP1b was derived primarily from Antarctica, as assumed in the construction of the ICE-nG sequence of models, has recently been directly confirmed on the basis of exposure age dating in coastal Antarctica (e.g. see Domack et al., 2005).

Acknowledgements

References

Adkins, J.F., Mclntyre, K., Schrag, D., 2002. The salinity, temperature and del-18O of the glacial deep ocean. Science 298, 1769–1773.

Al-Asfour, T.A., 1982. Changing sea level along the north coast of Kuwait Bay. Kegan Paul International Ltd., Boston 186pp (source of data for site KU in Fig. 3).

Bard, E., Hamelin, B., Fairbanks, R.G., Zindler, A., 1990. Calibration of the 14C timescale over the past 30,000 years using mass spectrometric U-Th ages from Barbados corals. Nature 345, 405–409.

Cato, I., 1992. Shore displacement data based upon lake isolations confirm the postglacial part of the Swedish Geochronological Timescale. Sveriges Geologiska Undersokoning, Ser. Ca 81, 75–80 (source of data for site AN of Fig. 3).

Chappell, J., Shackleton, N.J., 1986. Oxygen isotopes and sea level. Nature 324, 137–140.

Clark, J.A., Farrell, W.E., Peltier, W.R., 1978. Global changes in postglacial sea level: a numerical calculation. Quaternary Research 9, 265–287.

Clark, P.U., Mitrovica, J.X., Milne, G.A., Tamasea, M.E., 2002. Sea level fingerprinting as a direct test for the source of meltwater pulse 1a. Science 295, 2431–2438.

Denton, G.H., Hughes, T., 2002. Reconstructing the Antarctic ice sheet at the Last Glacial Maximum. Quaternary Science Reviews 21, 193–202.

Domack, Eugene, et al., 2005. Stability of the Larsen B ice shelf on the Antarctic Peninsula during the Holocene epoch. Science 436, 681–685.

Dubar, J.R., Anthony, E.J., 1995. Holocene environmental change and river mouth sedimentation in the Baie des Anges, French Riviera. Quaternary Research 43, 329–343 (source of data for site BA On Fig. 3).

Dyke, A.S., Andrews, J.T., Clarke, P.U., England, J.H., Milles, G.H., Milles, G.H., Shaw, J., Veillette, J., 2002. The Laurentide and Innuitian ice sheets during the Last Glacial Maximum. Quaternary Science Reviews 21, 9–31.

Fairbanks, R.G., 1988. Barbados offshore drilling program. LDGO Technical report L-DGO-88-2. 221 pp.

Fairbanks, R.G., 1989. A 17,000 year glacial euststic sea level record: influence of glacial melting rates on the Younger Dryas event and deep ocean circulation. Nature 342, 637–641.

Fairbanks, R.G., Dodge, R.E., 1979. Annual periodicity of the skeletal oxygen and carbon Stable isotopic composition in the coral Montastrea Annularis. Geochimica et Cosmochimica Acta 43 (7), 1–10.

Fairbanks, R.G., Charles, C.D., Wright, J.D., 1992. Origin of global meltwater pulses. In: Four Decades of Radiocarbon Studies (Long and Kra eds.), p. 473–500. Springer.

Fairbanks, R.G., Mortlock, R.A., Chiu, T.-C., Cao, L., Kaplan, A., Guilderson, T.P., Fairbanks, T.W., Bloom, A.L., Grootes, P.M., Nadeau, M.-J., 2005. Radiocarbon Calibration curve spanning 0 to 50,000 years BP based on paired 230Th/234U/238U and 14C dates on pristine corals. Quaternary Science Reviews 24 (16–17), 1781–1796.

Farrell, W.E., Clark, J.A., 1976. On postglacial sea level. Geophysical Journal of the Royal Astronomical Society 46, 647–667.

Hall, B.L., Denton, G.H., 1999. New relative sea level curves for the southern Scott Coast, Antarctica: Evidence for Holocene deglaciation of the western Ross Sea. Journal of Quaternary Science 14, 641–650 (source of data for site SC on Fig. 3).

Hanebuth, T., Statteger, K., Grootes, P.M., 2000. Rapid flooding of the Sunda shelf: a late glacial sea level record. Science 288, 1033–1035.

Huybrechts, P., 2002. Sea level changes at the LGM from ice dynamic reconstructions of the Greenland and Antarctic ice sheets during the glacial cycles. Quaternary Science Reviews 21, 203–231.

Kaye, C.A., Barghoorn, E., 1964. Late Quaternary sea level change and crustal rise in Boston, Massachussetts, with notes on the autocompaction of peat. Geological Society of American Bulletin 75, 63–80 (source of data for site BN on Fig. 3).

Lambeck, K., Chappell, J., 2001. Sea level changes through the last glacial cycle. Science 292, 679–686.

Lambeck, Kurt, Yokoyama, Yusuke, Purcell, Tony, 2002. Into and out of the Last Glacial Maximum: sea level change during oxygen isotope stages 3 and 2. Quaternary Science Reviews 22, 343–360.

Land, L.S., Lang, J.C., Smith, B.N., 1975. Preliminary observations on the carbon isotopic composition of some ref corals and symbiotic zooxanthellae. Limnology Oceanography 20, 283–287.

Martinsen, D.G., Pisias, N.G., Hays, J.D., Imbrie, J., Moore Jr., T.C., Shackleton, N.J., 1987. Age dating and orbital theory of the ice ages: development of a high resolution 0–300,000-year chronostratigraphy. Quaternary Research 27, 1–30.

Mitrovica, J.X., 2003. Recent controversies in predicting global sea level change. Quaternary Science Reviews 22, 127–133.

Mix, A., Ruddiman, W.F., 1984. Oxygen isotope analyses and Pleistocene ice volumes. Quaternary Research 21, 1–20.

Peltier, W.R., 1974. The impulse response of a Maxwell Earth. Reviews of Geophysics 12, 649–669.

Peltier, W.R., 1976. Glacial isostatic adjustement II: the inverse problem. Geophysical Journal of the Royal Astronomical Society 46, 669–706.

Peltier, W.R., 1982. Dynamics of the ice age Earth. Advances in Geophysics 24, 1–146.

Peltier, W.R., 1994. Ice age paleotopography. Science 265, 195–201.

Peltier, W.R., 1996. Mantle viscosity and ice age ice sheet topography. Science 273, 1359–1364.

Peltier, W.R., 1998a. postglacial variations in the level of the sea: implications for climate dynamics and solid Earth geophysics. Reviews of Geophysics 36, 603–689.

Peltier, W.R., 1998b. Implicit ice in the global theory of glacial isostatic adjustment. Geophysical Research Letters 25, 3957–3960 (see also for data for site HB on Fig. 3).

Peltier, W.R., 1999. Global sea level rise and glacial isoststic adjustment. Global and Planetary Change 20, 93–123.

Peltier, W.R., 2002a. On eustatic sea level history, Last Glacial Maximum to Holocene. Quaternary Science Reviews 21, 377–396.

Peltier, W.R., 2002b. Comments on the paper of Yokoyama et al. (2000) entitled ''Timing of Last Glacial Maximum from observed sea level minima''. Quaternary Science Reviews 21, 409–414.

Peltier, W.R., 2002c. Global glacial isostatic adjustment: paleo-geodetic and space geodetic tests Of the ICE-4G(VM2) model. Journal of Quaternary Science 17, 491–510.

Peltier, W.R., 2004. Global glacial isostasy and the surface of the ice age Earth: the ICE-5G(VM2) model and GRACE. Annual Review of Earth and Planetary Sciences 32, 111–149.

Peltier, W.R., 2005. On the hemispheric origins of meltwater pulse 1a. Quaternary Science Reviews 24, 1571–1655.

Peltier, W.R., Andrrews, J.T., 1976. Glacial isostatic adjustment I: the forward problem. Geophysical Journal of the Royal Astronomical Society 46, 605–646.

Peltier, W.R., Farrell, W.E., Clark, J.A., 1978. Glacial isostasy and relative sea level: A global finite element model. Tectonophysics 50, 81–110.

Peltier, W.R., Drummond, R., 2002. A ''broad shelf effect'' in he global theory of postglacial relative sea level history. Geophysical Research Letters 29, 1–2.

Pickerill, R.A., 1976. Evolution of coastal landforms of the Wairau Valley. New Zealand Geographer 32, 17–29 (source of data for site WV on Fig. 3).

Rostami, K., Peltier, W.R., Mangini, A., 2000. Quaternary marine terraces, sea level changes And uplift history of Patagonia, Argentina: Comparisons with predictions of the ICE-4G (VM2) model of the global process of glacial isostatic adjustment. Quaternary Science Reviews 19, 1495–1525.

Schimanski, A., Stattegger, K., 2005. Deglacial and Holocene evolution of the Vietnam shelf: Startigraphy, sediments and sea level change. Marine Geology 214, 365–387.

Seidov, D., Stouffer, R., Haupt, R.J., 2006. Is there a single bi-polar ocean sea saw? Global and Planetary Change, in press.

Shackleton, N.J., 1967. Oxygen isotope analyses and Pleistocene temperatures re-addressed. Nature 215, 15–17.

Shackleton, N.J., 2000. The 100,000 year ice age cycle identified and found to lag temperature, carbon dioxide, and orbital eccentricity. Science 289, 1897–1902.

Shennan, I., Innes, J.B., Long, A.J., Zong, Y., 1993. Late Devensian and Holocene relative sea level changes in northwest Scotland: new data to test existing models. Quaternary International 26, 97–123 (source of data for site AR on Fig. 3).

Shennan, I., Milne, G., 2003. Sea level observations around the Last Glacial Maximum From the Bonaparte Gulf, NW Australia. Quaternary Science Reviews 22, 1543–1547.

Tarasov, L., Peltier, W.R., 2004. A geophysically constrained large ensemble analysis of the deglacial history of the North American ice sheet complex. Quaternary Science Reviews 23, 359–388.

Waelbroeck, C., Labeyrie, L., Michel, E., Duplessy, J.-C., McManus, J., Lambeck, K., Balbon, E., Labracherie, M., 2002. Sea-level and deep water temperature changes derived from benthic foraminifera isotopic records. Quaternary Science Review 21, 295–305.

Weaver, A.J., Saenko, O.A., Clark, P.U., Mitrovica, J.X., 2003. Meltwater pulse 1a from Antarctica as a trigger for the Bølling-Allerød warm interval. Science 209, 1709–1713.

Weber, J.N., Deines, P., Weber, P.H., Baker, P.A., 1976. Depth and related changes in the C-13/C-12 ratio of skeletal carbonates deposited by the Caribbean reef-frame building coral Mantastrea annularis: further interpretations of chronological records preserved in the Corolla of corals. Paleobiol 1, 137–149.

Wu, P., Peltier, W.R., 1984. Pleistocene deglaciation and the Earth's rotation: A new analysis. Geophysical Journal of the Royal Astronomical Society 76, 202–242.

Yokoyama, Y., Lambeck, K., De Dekkar, P., Johnston, P., Fifield, L.K., 2000. Timing of Last Glacial Maximum from observed sea level minima. Nature 406, 713–716.

Yokoyama, Y., Lambeck, K., De Dekkar, P., Johnston, P., Fifield, L.K., 2001. Correction to Yokoyama et al. (2000). Nature 412, 99.